First Principles Study of Double Photoionization of H_2 Using Exterior Complex Scaling

[1]**T. N. Rescigno,** [2]**W. Vanroose,** [1]**D. A. Horner,** [3]**F. Martín,** [1,4]**C. W. McCurdy**

[1]Lawrence Berkeley National Laboratory, Chemical Sciences, Berkeley, CA 94720
[2]Departement Computerwetenschappen, Katholieke Universiteit Leuven, B-3001 Heverlee, Belgium
[3]Departamento de Química C-9, Universidad Autónoma de Madrid, 28049 Madrid, Spain.
[4]Departments of Applied Science and Chemistry, University of California, Davis, CA 95616

Abstract. Exterior complex scaling provides a practical path for first-principles studies of atomic and molecular ionization problems since it avoids explicit enforcement of asymptotic boundary conditions for 3-body Coulomb breakup. We have used the method of exterior complex scaling, implemented with both the discrete variable representation and B-splines, to obtain the first-order wave function for molecular hydrogen corresponding to a single photon having been absorbed by a correlated initial state. These wave functions are used to construct converged triple differential cross sections for double photoionization of aligned H_2 molecules.

1. Introduction

Double photoionization (DPI) — a process in which two electrons are ejected from an atomic or molecular target as the result of absorption of a single photon — is an exquisite tool for studying electron correlation. This stems from the fact that the process is controlled by the one-body dipole operator and hence cannot be accurately described with an independent particle description of either the target or the final-state dynamics. For the simplest case - that of atomic helium - the problem has been well studied both experimentally [1, 2, 3, 4, 5, 6, 7] and theoretically [8, 9, 10, 11, 12, 13] and much of the essential physics is now well understood. For the correspondingly "simple" two-electron molecule, H_2, the sudden removal of two electrons is followed by a "Coulomb explosion" of the resulting two bare protons. This latter process is generally slow on the scale of electronic motion, but rapid compared to molecular rotation. Therefore, the relative momentum vector of the dissociating nuclei defines the laboratory frame alignment of the molecule, while the magnitude of the nuclear kinetic energy release is correlated with the internuclear separation, *at the instant of photon absorption.* The experimental determination of differential ionization cross sections for such "fixed-in-space" molecules requires all four charged particles that emerge from the process to be measured in coincidence. Experiments of this type have been made feasible with the advent of "momentum imaging" detectors and several experiments on DPI of aligned molecular hydrogen have recently been

reported [14, 15, 16]. On the theoretical side, the problem has been modeled using approximate wave functions [17], atomic-like model calculations [18] and approximate parameterizations of the Triple Differential Cross Section (TDCS) cross section for double photoionization (TDCS) using models based on the atomic case [19]. But only recently has the problem been attacked using precise, nonperturbative quantum mechanical methods [20, 21] and the first TDCS for aligned H_2 were just reported [22]. Here we present a brief overview of the methods used to produce these TDCS, a sampling of the results obtained and some comparisons with available experiment.

2. Theoretical Approach

Single photon absorption, using first-order perturbation theory for the radiation field and the dipole approximation, is described by the driven Schrödinger equation,

$$(E_0 + \omega - H)|\Psi_{\rm sc}^+\rangle = \epsilon \cdot \mu \Psi_0 \tag{1}$$

where ϵ is the polarization unit vector, μ is the dipole operator for the electronic coordinates, and Ψ_0 is the initial (bound) state of the target. This equation must solved for the scattered wave $\Psi_{\rm sc}^+$ using purely outgoing wave boundary conditions. For a two-electron target, $\Psi_{\rm sc}^+$ contains asymptotic information that describes both single and double ionization processes.

The explicit application of proper outgoing wave scattering boundary conditions on $\Psi_{\rm sc}^+$ appropriate for double photoionization involves specification of the asymptotic form of the wave function for the three-body Coulomb breakup problem. Those boundary conditions, though well studied [23, 24], are awkward and complicated and have yet to prove useful in numerical computations as boundary conditions for solving the Schrödinger equation. An approach that has been successfully applied to electron impact- and photo double-ionization problems [25] is the "Exterior Complex Scaling" (ECS) method, since it avoids the explicit enforcement of asymptotic boundary conditions. In the ECS method, the radial coordinates of all the electrons are scaled by a complex factor, $\exp(i\eta)$ beyond some radius R_0:

$$r \to \begin{cases} r & \text{for } r \le R_0 \\ R_0 + (r - R_0)e^{i\eta} & \text{for } r > R_0 \end{cases} \tag{2}$$

This transformation, when applied to Eq. (1), simplifies the problem since it causes $\Psi_{\rm sc}^+$, which is a a purely outgoing wave, to decay exponentially for any $r_i > R_0$, while leaving it unchanged for $r_i \le R_0$. Solving Eq. (1) for the first order wave function under ECS, with R_0 chosen large enough to allow $\Psi_{\rm sc}^+(\mathbf{r}_1, \mathbf{r}_2)$ to reach its asymptotic form in the region where both coordinates are real valued, provides us with the physical wave function over the finite region where both coordinates are less than R_0.

The driven Schrödinger equation can be reduced to a set of linear algebraic equation by expanding the scattered wave and the initial target state in a discrete basis. Because the derivative of the scattered wave along the the ECS contour is discontinuous at R_0, it is important to choose a discretization scheme that can properly deal with this problem. ECS is most easily implemented by using numerical grid methods or with basis functions that have compact support so that the derivative discontinuity at R_0 can be handled exactly. Two such methods that work well in the present context are B-splines and finite elements with the discrete variable representation (FEM/DVR) that are scaled according to the ECS transformation. B-splines can be defined by setting a series of knots along the complex contour and

choosing one of the knot points to coincide with the ECS radius R_0. With FEM/DVR, we simply place the element boundaries along the contour, again placing one of the finite element boundaries at R_0.

B-splines were successfully used in our earlier studies of helium DPI and in our initial study of DPI of molecular hydrogen. We have since carried out an independent implementation using FEM/DVR. These two separate computational efforts provide a powerful check on the consistency of the results obtained and enable us to better assess the convergence of the final results. B-splines provide a flexible, rapidly convergent basis and their use allowed us to exploit a well developed existing technology [26, 27]. The FEM/DVR, in addition to providing an independent check on the results, has its own distinct computational properties. The Hamiltonian has a sparse structure in the DVR representation, making it easier to test for convergence of the single-center expansions by systematically increasing the number of partial waves used in the calculations.

With the scattered wave in hand, we need a procedure for extracting physical DPI scattering information, bearing in mind that the wave function is only known on a finite volume. This is accomplished by constructing the scattering amplitude which, apart from an irrelevant overall phase [25, 28], is given by the expression

$$f(\mathbf{k}_1,\mathbf{k}_2) = \left\langle \Phi^{(-)}(\mathbf{k}_1,\mathbf{r}_1)\Phi^{(-)}(\mathbf{k}_2,\mathbf{r}_2)\right| \left[E - T - v(\mathbf{r}_1) - v(\mathbf{r}_2)\right] \left|\Psi^{+}_{\rm sc}(\mathbf{r}_1,\mathbf{r}_2)\right\rangle , \tag{3}$$

where E is the excess energy above the DPI threshold, $\mathbf{k}_1$ and $\mathbf{k}_2$ are the momenta of the ejected electrons, T is the two-electron kinetic energy operator, $v(r)$ is the nuclear attraction potential seen by one electron in the field of the bare nuclei and the functions $\Phi^{(-)}(\mathbf{k},\mathbf{r})$ are H_2^+ continuum eigenfunctions with incoming momentum $\mathbf{k}$, which are solutions of the equation,

$$\left[\frac{k^2}{2} + \frac{\nabla^2}{2} + \frac{1}{|\mathbf{r}-\mathbf{A}|} + \frac{1}{|\mathbf{r}+\mathbf{A}|}\right] \Phi^{(-)}(\mathbf{k},\mathbf{r}) = 0\,, \tag{4}$$

and satisfy the usual relation, $\Phi^{(-)}(\mathbf{k},\mathbf{r}) = \left(\Phi^{(+)}(-\mathbf{k},\mathbf{r})\right)^*$. Eq. (4) can itself be converted into a driven equation for the scattered wave part of $\Phi^{(-)}$ which is solved using ECS [21]. We emphasize that the product $\Phi^{(-)}(\mathbf{k}_1,\mathbf{r}_1)\Phi^{(-)}(\mathbf{k}_2,\mathbf{r}_2)$ is *not* the physical final state wave function; the integral expression defined in Eq.(3) merely extracts the amplitude for double ionization from $\Psi^{+}_{\rm sc}$, as we have previously shown [25]. The choice of continuum H_2^+ eigenfunctions in the integral expression is crucial for our purposes because the orthogonality of the H_2^+ continuum states to the bound states of H_2^+ eliminates the contributions of the single ionization channels to Eq. (3). The TDCS for double photoionization is constructed from the amplitude according to

$$\frac{d^3\sigma}{dE_1 d\Omega_1 d\Omega_2} = \frac{4\pi^2}{\omega c} k_1 k_2 \left|f(\mathbf{k}_1,\mathbf{k}_2)\right|^2 . \tag{5}$$

The amplitude for double ionization, expressed as a six-dimensional volume integral in Eq. (3), can be rewritten using Gauss' theorem as a five-dimensional surface integral on a sphere of constant ρ in hyperspherical coordinates,

$$\begin{aligned} f(\mathbf{k}_1,\mathbf{k}_2) = \int d\Omega_1 \int d\Omega_2 \int d\rho \int_0^{\pi/2} d\alpha \; \frac{\rho^5 \sin^2\alpha \cos^2\alpha}{2} \\ \Phi^{(-)}(\mathbf{k}_1,\mathbf{r}_1)^* \Phi^{(-)}(\mathbf{k}_2,\mathbf{r}_2)^* \left[\frac{\overleftarrow{\partial}}{\partial\rho}\delta(\rho-\rho_0) - \delta(\rho-\rho_0)\frac{\overrightarrow{\partial}}{\partial\rho}\right] \Psi^{+}_{\rm sc}(\mathbf{r}_1,\mathbf{r}_2) \end{aligned} \tag{6}$$

where $\rho = \sqrt{r_1^2 + r_2^2}$ and $\tan\alpha = r_2/r_1$ and Ω_1 and Ω_2 are the normal spherical polar angles associated with the two electrons.

We proceed by using a single-center expansion of the full two-electron scattered wave function:

$$\Psi_{\rm sc}^{+M}(\mathbf{r}_1,\mathbf{r}_2) = \sum_{\mu_1\mu_2,j_1\geq j_2} \left(\frac{\psi^{\rm dir}_{j_1\mu_1,j_2\mu_2}(r_1,r_2)}{r_1 r_2} Y_{j_1\mu_1}(\hat{\mathbf{r}}_1) Y_{j_2\mu_2}(\hat{\mathbf{r}}_2) + \frac{\psi^{\rm exch}_{j_1\mu_1,j_2\mu_2}(r_1,r_2)}{r_1 r_2} Y_{j_2\mu_2}(\hat{\mathbf{r}}_1) Y_{j_1\mu_1}(\hat{\mathbf{r}}_2) \right), \tag{7}$$

where the superscript M denotes that $M = \mu_1 + \mu_2$ is a good quantum number, which is further restricted to the values $(0, \pm 1)$ by dipole selection rules. For the H_2^+ scattering eigenstates, we use a single-center expansion of the form

$$\Phi^{(+)}(\mathbf{k},\mathbf{r}) = \left(\frac{2}{\pi}\right)^{1/2} \sum_{l,m} i^l e^{i\eta_l(k)} Y^*_{lm}(\hat{\mathbf{k}}) \sum_{l'} \left(\frac{\phi^{(c)}_{l,k}(r)}{kr}\delta_{l,l'} + \frac{R^{lm}_{l'}(r)}{r} \right) Y_{l'm}(\hat{\mathbf{r}}), \tag{8}$$

where $\phi^{(c)}_{l,k}(r)$ is the radial Coulomb wave function for $Z = 2$ and $\eta_l(k)$ is the usual Coulomb phase shift. The unknown radial functions $\psi^{\rm dir}_{j_1\mu_1,j_2\mu_2}(r_1,r_2)$, $\psi^{\rm exch}_{j_1\mu_1,j_2\mu_2}(r_1,r_2)$ and $R^{lm}_{l'}(r)$ are in turn obtained from the solution of the coupled linear equations that result when Eqs. (1) and (4) are expanded in B-spline or FEM/DVR functions. Substitution of Eqs. (7) and (8) into Eq. (6) gives the following expression for the DPI amplitude:

$$f^{(M)}(\mathbf{k}_1,\mathbf{k}_2) = \sum_{l_1,\mu_1}\sum_{l_2,\mu_2} \left(\frac{2}{\pi}\right) i^{-l_1-l_2} e^{i\eta_{l_1}(k_1)+i\eta_{l_2}(k_2)} \Big[Y_{l_1\mu_1}(\hat{\mathbf{k}}_1) Y_{l_2\mu_2}(\hat{\mathbf{k}}_2) \sum_{j_1\geq j_2} F^{\rm dir}_{l_1 l_2 j_1\mu_1 j_2\mu_2}(k_1,k_2)\Delta_{j_1 l_1}\Delta_{j_2 l_2} + Y_{l_1\mu_2}(\hat{\mathbf{k}}_1) Y_{l_2\mu_1}(\hat{\mathbf{k}}_2) \sum_{j_1\geq j_2} F^{\rm exch}_{l_1 l_2 j_1\mu_1 j_2\mu_2}(k_1,k_2)\Delta_{j_2 l_1}\Delta_{j_1 l_2} \Big], \tag{9}$$

where the factor $\Delta_{j,l}$, which is unity if $j+l$ is even and zero otherwise, results from the homonuclear symmetry of the target. The direct radial amplitude in this expression is the one-dimensional surface integral,

$$F^{\rm dir}_{l_1,l_2,j_1,\mu_1,j_2,\mu_2}(k_1,k_2) = \frac{\rho_0}{2}\int_0^{\pi/2} d\alpha \left(\frac{\phi^{(c)}_{l_1,k_1}(r_1)}{k_1}\delta_{l_1,j_1} + R^{l_1\mu_1}_{j_1}(r_1) \right) \left(\frac{\phi^{(c)}_{l_2,k_2}(r_2)}{k_2}\delta_{l_2,j_2} + R^{l_2\mu_2}_{j_2}(r_2) \right) \left[\frac{\overleftarrow{\partial}}{\partial\rho} - \frac{\overrightarrow{\partial}}{\partial\rho} \right]_{\rho=\rho_0} \psi^{\rm dir}_{j_1\mu_1,j_2\mu_2}(r_1,r_2), \tag{10}$$

and the corresponding exchange amplitude is obtained by interchanging j_1, μ_1 and j_2, μ_2 on the r.h.s. in the test functions (but not in the wave function,$\psi^{\rm exch}_{j_1\mu_1,j_2\mu_2}$).

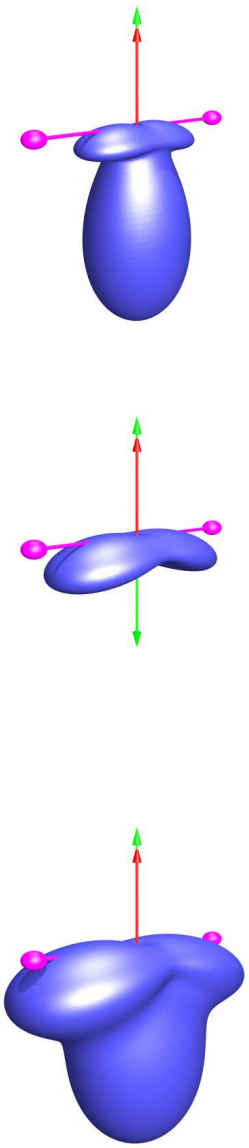

Figure 1. Color online. 3D plots of TDCS where fixed electron, aligned along polarization direction, is perpendicular to the molecule and has 10% (upper panel), 50% (middle panel) and 90% (lower panel) of the available energy.

3. Results

All of the calculations reported here were carried out at the equilibrium internuclear distance $R_{\rm eq} = 1.40$ bohr for a photon energy of 75 eV. Calculations were made using two independent sets of codes using B-splines and FEM/DVR, respectively, and the

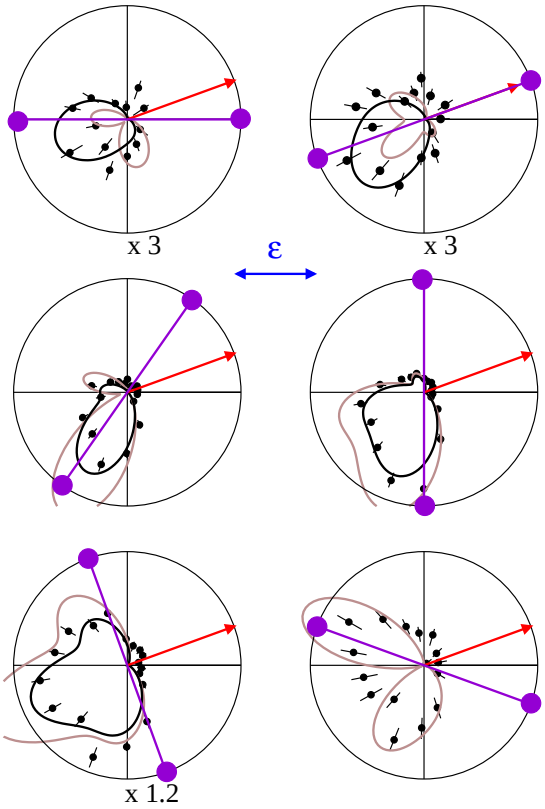

Figure 2. Color online. Comparison with experiments of Weber (Fig. 5.75 of ref. [29]). The fixed electron (arrow), with 90% of the available energy is 20° to the polarization direction (horizantal). The molecule is oriented (left to right, starting at top row) at 0°, 20°, 55°, 90°, 110° and 160° to the polarization direction. Current results are shown unaveraged (light solid curves) and averaged over experimental acceptance angles (black solid curves).

results were found to agree very well. By systematically increasing the number of partial waves used in the calculations, we found that with $l_{\max} = 7$ the results were fully converged and that the dipole length and velocity gauges gave virtually identical results.

It has been pointed out that, when averaged over molecular orientations, the TDCS patterns for molecular hydrogen are very similar to those for helium [30] and that model calculations work rather well in describing that behavior. This is not the case, however, for aligned H_2, where the TDCS reveal striking effects of an entirely molecular nature, such as pronounced changes in the patterns of electron ejection that depend on the orientation of the molecular axis with respect to the photon polarization. Some of these effects can be explained as resulting from the fact that the Σ contribution to DPI in H_2 is much smaller than the Π contribution, but there are clearly other cases that have no such simple explanation. An example of such a purely molecular effect is displayed in the three dimensional plots of the TDCS shown in Fig. 1 for three different energy sharings of the fixed and plotted electrons, in the case where the fixed electron lies along the direction of polarization. We note that for equal energy

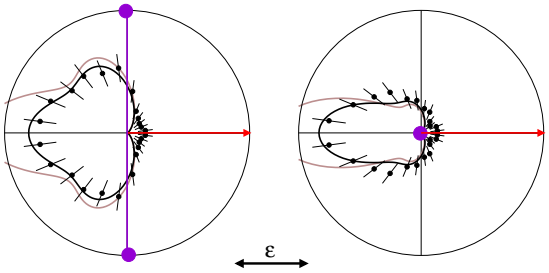

Figure 3. Color online. Comparison with experiments of Weber (Figs. 5.71a and 5.73a of ref. [29] and ref. [32]). The fixed electron (arrow), with 90% of the available energy, is aligned with the polarization direction (horizantal). The molecule is perpendicular to the polarization direction, either in the plane of the measured electron (left) or perpendicular to it (right). Current results are shown unaveraged (light solid curves) and averaged over experimental acceptance angles (black solid curves).

sharing (middle panel), the selection rule that produces zero for back-to-back ejection of the photoelectrons is still preserved [31], but that the cylindrical symmetry about the polarization axis that would be present in the atomic case is clearly absent in the molecular case. Moreover, this is not a consequence of the different magnitudes of the Σ and Π contributions, since there is no contribution from Σ to the TDCS when the polarization is perpendicular to the molecular axis.

In order to meaningfully compare theoretical calculations with experiments on this system, one must take account of the fact that the latter all involve finite ranges of acceptance for the angles of the fixed electron, plotted electron and molecule, as well as finite resolution for the energy sharing between the two electrons. The fixed-nuclei TDCS must therefore be averaged over the finite ranges of the various observables to compare with the measured quantities. For example, in the experiments of Weber shown in Fig. 2, a plane is defined by the fixed electron and the direction of polarization. Angle ranges refer to in-plane and out-of-plane angles with the analogy to a globe with the plane at the equator. In-plane angles refer to rotation in the plane (longitude) with all angles equally weighted. The out of plane angles are weighted by a factor of $\sin(\phi)$. Typical acceptance ranges for the experiments of Weber range from $\pm 12^\circ$ for the electrons to $\pm 45^\circ$ for the molecule. The exact values are given in ref. [29] for the figures cited below.

In Fig. 2, we show a comparison between theory and experiment for an "in-plane" case with unequal energy sharing, where the fixed electron makes an angle of 20° with the polarization direction and the molecule rotates in the same plane. Since the experimental results of Weber are reported in arbitrary units but are internormalized, we have chosen a single scaling factor that gives the best overall fit to our averaged data. We see that while proper averaging of the calculated TDCS is clearly necessary to achieve good agreement with experiment, averaging obscures some of the interesting detail of the TDCS. We have found similarly good agreement (not shown) between suitably averaged theoretical results and the in-plane experimental results of Gisselbrecht *et al.* [16] reported for equal energy sharing.

Another comparison with experiment is shown in Fig. 3. This is a pure Π_u case (for the unaveraged theory) where the molecule is perpendicular to the polarization, while the fixed electron and the polarization direction form a common axis about

which there would be cylindrical symmetry in the case of helium. In the molecular case, however, the cylindrical geometry of the atomic case becomes flattened along the direction of the molecular axis. While the effect is more clearly seen in the unaveraged results, it is also evident in the averaged results and in the experimental measurements.

4. Conclusions

We have built the computational tools needed to carry out precise quantum mechanical calculations of H_2 double photoionization and have demonstrated that the calculations are converged. We have also provided a consistency check on the results by implementing the ECS formalism with two different numerical approaches. Clear molecular effects are visible in the calculated TDCS and a range of sensitively varying shapes for these cross sections emerge when different geometries of photoejection are explored. While agreement between theory and experiment is generally good, we have found that the averaging needed to mimic the finite acceptance angles of the experiments can obscure finer details of the TDCS. It is also our hope that theory will provide a useful tool to guide experiment in looking for the most interesting geometries.

Acknowledgments

This work was performed at the University of California Lawrence Berkeley National Laboratory under the auspices of the US Depart1ment of Energy under contract DE-AC02-05CH11231 and was supported by the U.S. DOE Office of Basic Energy Sciences, Division of Chemical Sciences. FM is supported by the DGI (Spain) project No. BFM2003-00194.

[1] Wehlitz R, Heiser F, Hemmers O, Langer B, Menzel A and Becker U 1991, *Phys. Rev. Lett.* **67** 3764
[2] Braüning M, Dörner R, Cocke C L, Prior M H, Kriässig B, Kheifets A S, Bray I, Braüning-Demian A, Carnes K, Dreuil S, Mergel V, Richard P, Ulrich J and Schmidt-Böcking H 1988 *J. Phys. B: At. Mol. Opt. Phys.* **31** 5149
[3] Mergel V, Achler M, Dörner R, Khayyat K, Kambara T, Awaya Y, Zoran V, Nyström B, Spielberger L, McGuire J H, Feagin J, Berakdar J, Azuma Y and Schmidt-Böcking H 1989 *Phys. Rev. Lett.* **80** 5301
[4] Samson J A R, Stolte W C, He Z X, Cutler J N and Lu Y 1998 *Phys. Rev. A* **57** 1906
[5] Weightman J P, Cvejanovi'c S and Reddish T J 1998 *J. Phys. B: At. Mol. Opt. Phys.* **31** 1753
[6] Soejima K, Danjo A, Okuno K and Yagishita A 1999 *Phys. Rev. Lett.* **83** 1546
[7] Huetz A and Mazeau J 2000 *Phys. Rev. Lett.* **85** 530
[8] J.Colgan, Pindzola M S and Robicheaux F 2001 *J. Phys. B* **34** L457–L466
[9] Selles P, Malegat L and Kazansky A K 2002 *Phys. Rev. A* **65** 032711
[10] Kheifets A S and Bray I 2002 *Phys. Rev. A* **65** 022708
[11] Malegat L, Selles P and Huetz A 1997 *J. Phys. B: At. Mol. Opt. Phys.* **30** 251
[12] Huetz A, Selles P, Waymel D and Mazeau J 1991 *J. Phys. B: At. Mol. Opt. Phys.* **24** 1917
[13] McCurdy C W, Horner D A, Rescigno T N and Martín F 2004 *Phys. Rev. A* **69** 032707
[14] T. Weber, *et al.* 2004 *Nature* **431** 437
[15] Th. Weber, *et al.* 2004 *Phys. Rev. Lett.* **92** 163001
[16] M. Gisselbrecht *et al.* 2006 *Phys. Rev. Lett.* **96** 153002
[17] Walter M and Briggs J 1999 *J. Phys. B.* **32** 2487
[18] Kheifets A S 2005 *Phys. Rev. A* **71** 022704
[19] Reddish T J and Feagin J M 1999 *J. Phys. B.* **32** 2473
[20] Colgan J, Pindzola M S and Robicheaux F 2004 *J. Phys. B.* **37** L377
[21] Vanroose W, Martín F, Rescigno T N and McCurdy C W 2004 *Phys. Rev. A* **70** 050703
[22] Vanroose W, Martín F, Rescigno T N and McCurdy C W 2005 *Science* **310** 1787
[23] Alt E O and Mukhamedzhanov A M 1993 *Phys. Rev. A* **47** 2004
[24] Kadyrov A S, Mukhamedzhanov A M, Stelbovics A T and Bray I 2004 *Phys. Rev. A* **70** 062703

[25] McCurdy C W, Baertschy M and Rescigno T N 2004 *J. Phys. B* **37** R137
[26] Martín F 1999 *J. Phys. B* **32** R197–R231
[27] Bachau H, Cormier E, Decleva P, Hansen J E and Martín F 2001 *Rep. Prog. Phys.* **64** 1815–1942
[28] Rescigno T N, Baertschy M and McCurdy C W 2003 *Phys. Rev. A* **68** 020701
[29] Weber T PhD thesis Institut fuer Kernphysik, Frankfurt 2003 available at http://hsb.uni-frankfurt.de/web/publications/diplom_doktor/
[30] D. P. Seccombe, *et al.* 2002 *J. Phys. B* **35** 3767
[31] Walter M and Briggs J 2000 *J. Phys. B.* **32** 1630
[32] Th. Weber, private communication (2006).